MATERIALS SCIENCE / МАТЕРИАЛОВЕДЕНИЕ

UDC 621.791.927.5
DOI 10.17073/0368-0797-2023-6-709-717

Original article
Оригинальная статья

Structure and mechanical properties anisotropy of a steel product manufactured by layer-by-layer electric arc wire 3D printing

I. V. Vlasov ✉, **A. I. Gordienko, A. E. Kuznetsova, V. M. Semenchuk**

Institute of Strength Physics and Materials Science, Siberian Branch of Russian Academy of Sciences (2/4 Akademicheskii Ave., Tomsk 634055, Russian Federation)

✉ viv@ispms.ru

Abstract. The work presents the study of structure and mechanical properties anisotropy of a metal wall obtained using electric arc wire 3D printing (WAAM) with ER70S-6 wire. The layers were deposited in the protective gases of carbon dioxide and argon. As a result of structural studies, it was found that the internal structure of the model product in form of a wall can be divided into three zones. Repeated heating, cooling cycles and degree of accumulated heat influence the formation of different wall zones. As a result of rapid heat removal to the substrate during deposition of the first layers, the wall base (zone *1*) contains large elongated grains with acicular ferrite structure. The wall middle part (zone *2*) consists of ferrite-pearlite structure, which was formed as a result of recrystallization under conditions of repeated heating and cooling during 3D printing. The size of ferrite grains in zone *2* varies from 11 to 16.3 μm with increasing the number of layers. The gradual accumulation of heat during 3D printing led to the formation of structures in zone *3* under conditions of overheating and a reduced cooling rate. As a result, the wall upper part (zone *3*) consists of large ferrite grains (up to 29.8 μm), sorbite, and a small proportion of Widemanstatten ferrite and acicular ferrite. It is shown that the most uniform level of mechanical characteristics ($\sigma_{0.2}$ = 340 MPa, σ_u = 470 MPa, ε = 28 %) correspond to the samples cut from zone *2* in a direction parallel to 3D printing direction. The samples cut in the vertical direction relative to 3D printing and from zone *3* show the lowest level of microhardness and mechanical characteristics ($\sigma_{0.2}$ = 260 MPa, σ_u = 425 MPa, ε = 20 %).

Keywords: additive technology, WAAM, GMAW, engineering steel, microstructure, mechanical properties, thermal cycling

Acknowledgements: The work was performed within the framework of the state task of the Institute of Strength Physics and Materials Science, Siberian Branch of Russian Academy of Sciences, project No. FWRW-2021-0009.

For citation: Vlasov I.V., Gordienko A.I., Kuznetsova A.E., Semenchuk V.M. Structure and mechanical properties anisotropy of a steel product manufactured by layer-by-layer electric arc wire 3D printing. *Izvestiya. Ferrous Metallurgy*. 2023;66(6):709–717.
https://doi.org/10.17073/0368-0797-2023-6-709-717

Исследование структуры и анизотропии механических свойств стального изделия, полученного методом послойной электродуговой проволочной 3D-печати

И. В. Власов ✉, **А. И. Гордиенко, А. Е. Кузнецова, В. М. Семенчук**

Институт физики прочности и материаловедения Сибирского отделения РАН (Россия, 634055, Томск, пр. Академический, 2/4)

✉ viv@ispms.ru

Аннотация. В работе проведено исследование структуры и анизотропии механических свойств металлической стенки, полученной с помощью электродуговой проволочной 3D-печати (WAAM) проволокой ER70S-6. Нанесение слоев проводится в среде защитных газов: углекислого газа и аргона. В результате структурных исследований обнаружено, что внутреннюю структуру сформированного модельного изделия в виде элементарной стенки можно разделить на три зоны. Формирование разных зон стенки обусловлено многократными циклами нагрева и охлаждения участков стенки и степенью накопленного тепла по мере увеличения циклов 3D-печати. В результате быстрого теплоотвода в подложку при нанесении первых слоев основание стенки (зона *1*) содержит крупные вытянутые зерна со структурой игольчатого феррита. Средняя часть стенки (зона *2*) состоит из феррито-перлитной структуры, которая формируется

в результате перекристаллизации в условиях многократного нагрева и охлаждения при 3D-печати. Размер ферритных зерен в зоне *2* изменяется в пределах от 11 до 16,3 мкм по мере увеличения количества слоев. Постепенное накопление тепла при 3D-печати приводит к формированию структур в зоне *3* в условиях перегрева и сниженной скорости охлаждения, вследствие этого верхняя часть стенки (зона *3*) состоит из крупных ферритных зерен (размером до 29,8 мкм), сорбита, небольшой доли виндманштеттового и игольчатого феррита. Однородное распределение микротвердости и оптимальные механические характеристики ($\sigma_{0,2}$ = 340 МПа, $\sigma_в$ = 470 МПа, ε = 28 %) соответствует образцам, вырезанным из зоны *2* в направлении, параллельном 3D-печати. Образцы, вырезанные в вертикальном направлении относительно 3D-печати из зоны *3*, демонстрируют самые низкие микротвердость и механические характеристики ($\sigma_{0,2}$ = 260 МПа, $\sigma_в$ = 425 МПа, ε = 20 %).

Ключевые слова: аддитивная технология, WAAM, GMAW, конструкционная сталь, микроструктура, механические свойства, термоциклирование

Благодарности: Работа выполнена в рамках государственного задания Института физики прочности и материаловедения Сибирского отделения РАН, тема номер FWRW-2021-0009.

Для цитирования: Власов И.В., Гордиенко А.И., Кузнецова А.Е., Семенчук В.М. Исследование структуры и анизотропии механических свойств стального изделия, полученного методом послойной электродуговой проволочной 3D-печати. *Известия вузов. Черная металлургия*. 2023;66(6):709–717. https://doi.org/10.17073/0368-0797-2023-6-709-717

Introduction

Over the past few decades, there has been active development in additive manufacturing of products and the restoration of machine parts using this technology [1]. Additive technologies are in high demand in aviation, the space industry, medicine, and mechanical engineering, and their application is economically feasible for manufacturing prototypes and small-batch production. These technologies are unique and indispensable, particularly for producing parts with complex internal geometry, where the addition of internal stiffeners, the creation of channel systems inside the product, or the manufacturing of parts with minimal loss of expensive raw materials is essential [2]. Currently, various technologies for additive manufacturing of metal parts can be distinguished, including powder-based methods such as selective laser melting, direct laser deposition, and plasma-transferred arc hardfacing, as well as wire-based methods like electron beam wire-feed additive manufacturing and wire and arc additive manufacturing (WAAM) [3].

The WAAM process in a shielding gas environment (GMAW) is the most common, high-performance, cost-effective, and simple technology. This process offers rapid deposition rates of about 4 – 9 kg/h [4] and enables the creation of complex dimensional structures.

The technology of material deposition with a consumable electrode in the environment of shielding inert (MIG) or active (MAG) gases allows the deposition of a wide range of metals, including layer-by-layer deposition of difficult-to-machine alloys such as titanium [5; 6]. In some cases, subsequent heat treatment is required to obtain specified mechanical properties. Each layer in the 3D printing process undergoes multiple thermal heatings that attenuate when moving away from the place of a new layer deposition. All layers are unique as heat accumulates in the wall while heat removal is insufficient [7]. Consequently, the thermal history is shaped, leading to structural-phase transformations and alterations in internal stresses [8]. Uncontrolled thermal impact can pose a significant challenge for alloys requiring multi-stage heat treatment [9].

Another critical issue is the anisotropy of mechanical properties. The growth of columnar crystals during 3D printing, directed heat removal during cooling, the formation of layer boundaries, and the varying thermal stresses experienced by each layer result in heterogeneous mechanical properties in different cross-sections of the product [10]. This anisotropy in mechanical properties significantly complicates the process of designing and obtaining volumetric items with specified parameters.

The objective of this study was to investigate the features of structure formation during 3D printing with structural steel wire and its impact on the distribution of mechanical properties in different sections of the product.

Materials and methods

A copper-coated ER70S-6 wire with a diameter of 1.2 mm was utilized for layer-by-layer 3D printing. As a substrate, we employed steel of 09G2S grade with a similar chemical composition, designed for the production of parts and elements in welded structures. The substrate was 10 mm thick and was selected to minimize thermal distortion during the 3D printing process. The chemical composition of the materials is provided in Table 1.

Metal wire deposition was carried out using a system comprising a FANUC AM-100iD multi-axis mechanized manipulator (Fig. 1, *a*) integrated with an EWM Titan XQ R 400 welding machine. The wire was deposited in GMAW mode by the MAG method, employing a mixture of carbon dioxide and argon in a ratio of 82 % Ar and 18 % CO_2. The optimal 3D printing parameters were pre-selected based on the synergistic curves provided by the manufacturer. This selection aimed to ensure stable arcing, minimal spattering, and the deposition of even layers.

Table 1

Chemical composition of 09G2S substrate and ER70S-6 wire

Таблица 1. **Химический состав материала подложки 09Г2С и проволоки ER70S-6**

Material	Element content, wt. %							
	C	Si	Mn	Ni	Cr	Cu	P/S/N	Fe
09G2S	up to 0.12	0.5 – 0.8	1.3 – 1.7	up to 0.30	up to 0.30	up to 0.30	up to 0.01	≈96.8
ER70S-6	0.06 – 0.10	0.9 – 1.1	1.6 – 1.8	up to 0.02	up to 0.02	up to 0.02	up to 0.01	≈96.4

The most common structural element is the vertical wall, which was produced using 3D printing by depositing layers, each 100 mm long, in 50 passes. Layers were deposited at regular intervals (30 s) with a slight horizontal shift (2 mm) to increase the width of the wall. The welding torch was tilted at a 10° angle against the substrate, moved "backhand". The distance between the torch tip and the workpiece was approximately 10 – 12 mm.

The scheme for cutting samples from the wall is illustrated in Fig. 1, *b*. To conduct microstructural studies, a cross-section of the wall (highlighted in gray in Fig. 1, *b*) was fabricated, encompassing the substrate itself. This facilitated additional analysis of the microstructure in the heat-affected zone. The structural analysis of the samples was conducted using the Carl Zeiss Axiovert 25 microscope and LEO EVO 50 scanning electron microscope at the Nanotech Center for Collective Use of the Institute of Strength Physics and Materials Science, Siberian Branch, RAS. The ferrite grain size was determined using the method of counting intersections of grain boundaries (GOST 5639 – 82). Tensile samples were extracted from both the substrate and the wall, in both horizontal (from the top and bottom of the wall) and vertical directions relative to the 3D printing. The working part of the double-bladed shaped samples had dimensions of 4.0×1.5×40 mm. Static tensile tests were conducted on an Instron 5582 electromechanical machine with a crosshead travel speed of 0.6 mm/min. Microhardness was assessed using a PTM-3 device with a load on the Vickers pyramid of 0.98 N (100 g).

Research results

Microstructural studies

Following 3D printing in the GMAW print mode, the wall was successfully formed. The geometric characteristics of the wall include a height of 66 mm, a width ranging from 9.7 to 10.4 mm; and a 2 mm recess in the substrate.

Macroanalysis of the outer surface of the wall revealed that in the lower part, the boundaries between the layers are smooth and clear (Fig. 1, *c*). However, towards the top of the wall (approximately from its middle), undulating layer boundaries are formed.

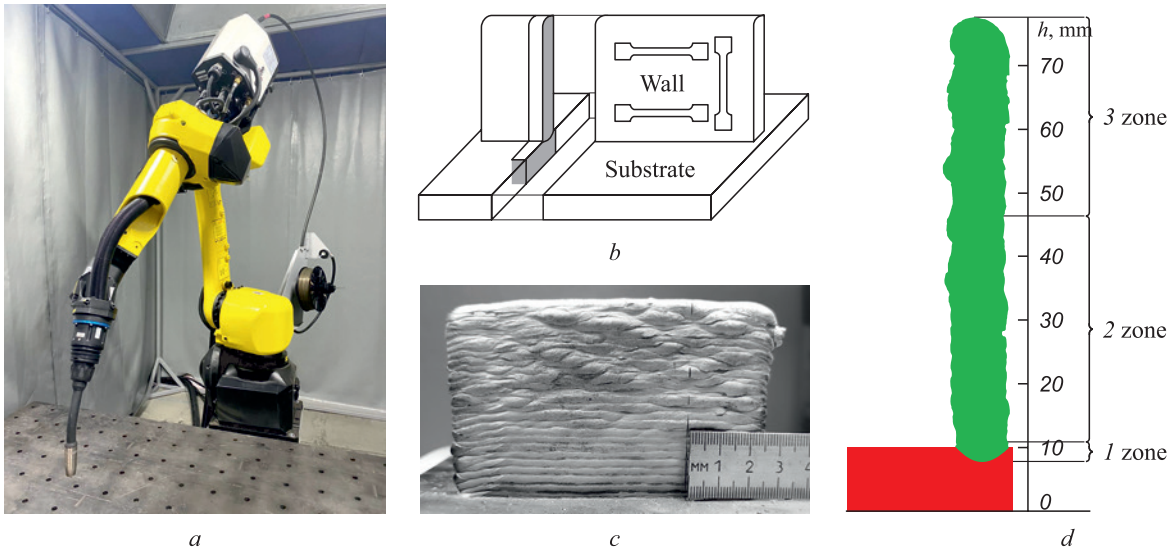

Fig. 1. Photograph of the FANUC ARC Mate-100iD multi-axis robot (*a*), samples cutting scheme (*b*), the wall photograph (*c*), the wall zones scheme (*d*)

Рис. 1. Фотография многоосевого робота FANUC ARC Mate-100iD (*a*), схема вырезки образцов (*b*), фотография стенки (*c*) и схема зон в стенке (*d*)

The 09G2S steel substrate exhibited a ferrite-perlite structure with pronounced banding in the rolling direction (Fig. 2, *a*). The average ferrite grain size was 18 ± 1 μm. In the heat-affected zone, the steel structure transitions from bainitic to ferrite-pearlitic (Fig. 2, *b*).

In the cross-section of the printed wall, three distinct zones can be identified, as illustrated in Fig. 1, *d*. The dimensions of zones *1*, *2*, and *3* were 3 mm (4 %), 35 mm (52 %), and 30 mm (44 %), respectively. It is worth noting that the sum of all zones exceeds the wall height due to zone *1* incorporating a portion of the melted substrate (Fig. 1, *c*).

Zone *1*, located at the base of the wall and the boundary layer with the substrate, is approximately 3 mm in height. It consists of large elongated columnar-shaped grains (Fig. 2, *d*). Allotriomorphic ferrite formed along the boundaries of former austenitic grains, with acicular ferrite developing inside the grains.

Zone *2* situated in the middle part of the wall, is approximately 35 mm in height and is characterized by ferrite grains with pearlite inclusions (Fig. 2, *e*). The average ferrite grain size in this zone varies from 11 ± 1 μm in the lower part of zone *2* to 16.3 ± 2 μm in the upper part, relative to the wall height.

Zone *3*, located in the upper part of the wall, is approximately 30 mm in height and comprises non-equiaxial ferrite grains, Widmanstätten ferrite, separate regions with acicular ferrite, and a pearlitic component (Fig. 2, *f*). The average size of ferrite grains in this zone is significantly larger, measuring 29.8 ± 2 μm.

At the microstructural level, the boundaries between the zones within the wall are not distinctly defined. The transitions between them are seamless and often occupy a substantial portion of the overall area.

The pearlite component and its distribution in the wall structure were examined in greater detail using a scanning

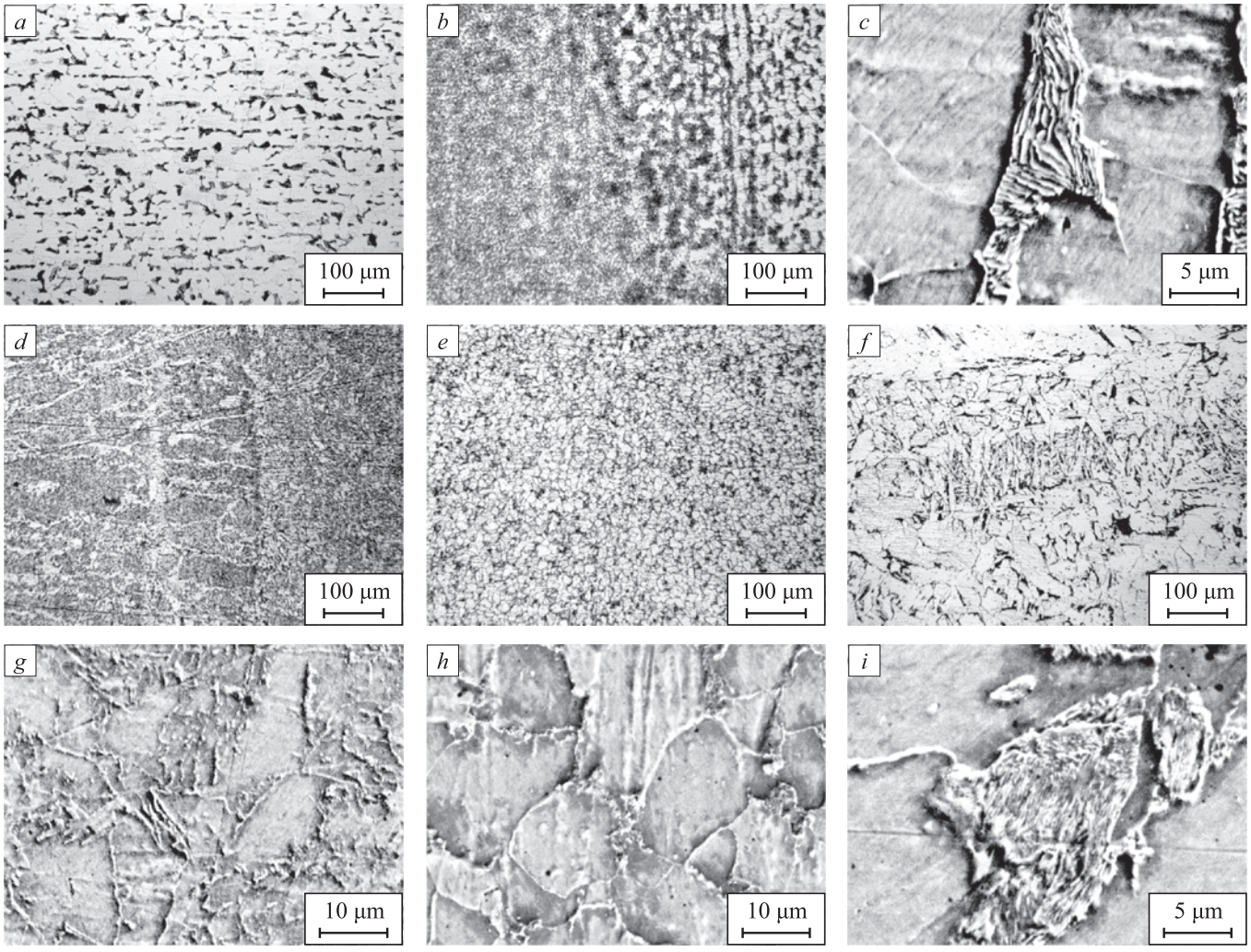

Fig. 2. Optical (*a*, *b*, *d* – *f*) and SEM (*c*, *g* – *i*) photographs of the substrate microstructure (*a* – *c*), the wall base (zones *1*) (*d*, *g*), the wall middle part (zones *2*) (*e*, *h*), the wall top parts (zone *3*) (*f*, *i*)

Рис. 2. Оптические (*a*, *b*, *d* – *f*) и РЭМ (*c*, *g* – *i*) фотографии микроструктуры подложки (*a* – *c*), основания стенки (зоны *1*) (*d*, *g*), средней части стенки (зоны *2*) (*e*, *h*), верхней части стенки (зоны *3*) (*f*, *i*)

electron microscope (Fig. 2, *c*, *h* – *i*). In the 09G2S steel substrate, lamellar pearlite with an interlamellar spacing of about 0.4 ± 0.04 μm was identified (Fig. 2, *c*). As the fusion boundary with the wall was approached, granular pearlite formed in the heat-affected zone. This granular pearlite is likely a result of insufficient austenitization during the short-term heating of the substrate, leading to an inhomogeneous carbon concentration in austenite.

No areas of pearlite were found in zone *1*. Instead, individual cementite particles and thin interlayers were observed near the boundaries of former austenitic grains and acicular ferrite (Fig. 2, *h*). In zone *2*, granular pearlite was observed, distributed along the ferrite grain boundaries (Fig. 2, *i*).

In zone *3*, the distribution of the pearlite component is heterogeneous. As one moves away from zone *2*, the proportion of granular pearlite in the structure decreases, and lamellar pearlite is formed instead (Fig. 2, *i*). The interlamellar spacing in the lamellar pearlite in zone *3* is 0.25 ± 0.03 μm, corresponding to the sorbite structure. In the upper part of the wall, within a distance of up to 3 mm from its top, the proportion of the pearlitic component decreases.

Microhardness measurement

Microhardness measurements were conducted on the cross-section of the wall (Fig. 3, *a*). The origin on the abscissa corresponds to the rear part of the substrate (as depicted in Fig. 1, *d*). The microhardness of the substrate material was recorded as 1.6 GPa. In the heat-affected zone (~7 mm), microhardness initially decreased to 1.35 GPa and then returned to the initial values of the substrate material microhardness. As the fusion boundary is approached, microhardness increases in zone *1*. The acicular ferrite structure in zone *1* exhibits the highest microhardness values, reaching approximately 1.8 GPa. Given the limited length of this zone (Fig. 3, *a*), the graph only displays a portion of the measured points.

In zone *2* and partially in zone *3*, microhardness gradually decreases, with a more intensive reduction and greater spread of values observed in zone *3*. As the upper boundary of the wall is approached, microhardness increases from 1.3 to 1.5 GPa.

Static tensile tests

Static tensile tests were conducted on samples cut in both horizontal (from the bottom and top of the wall) and vertical directions relative to 3D printing (Fig. 1, *b*). The need to test samples from the lower (zone *2*) and upper (zone *3*) parts of the wall arises from differences in both the macrogeometry of the layers (presence of undulating layer boundaries in zone *3*) and the microstructure in zones *2* and *3*.

In this study, the substrate and reference data on the mechanical properties of the ER70S-6 wire served as the baseline for evaluating the mechanical properties of the wall. The samples cut in the vertical and horizontal directions (from zone *3*) relative to 3D printing exhibit the lowest strength characteristics, even when compared to the substrate material (Fig. 3, *b*; Table 2). Simultaneously, the values of yield strength and tensile strength are close, but the plasticity of the samples from the vertical section is lower. Samples from the lower part of the wall (zone *2*) exhibit higher strength properties and are closer to the reference values of the wire's mechanical properties.

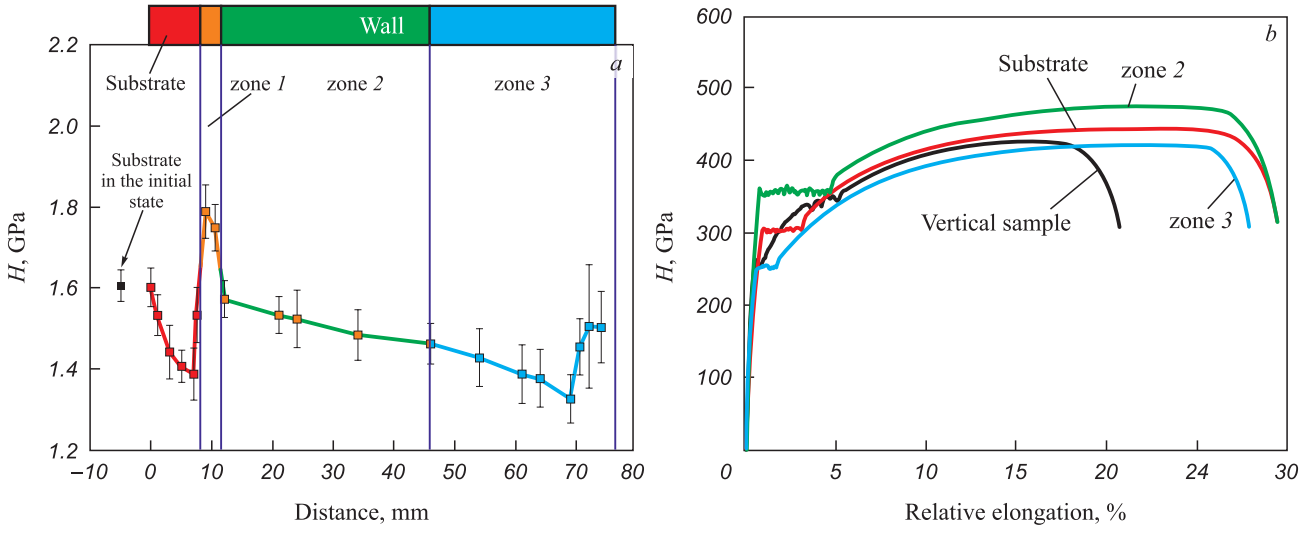

Fig. 3. Microhardness of the wall cross-section measured by its height (*a*), graphs of static tension (*b*)

Рис. 3. Микротвердость в поперечном сечении стенки, измеренная по ее высоте (*b*), диаграммы статического растяжения (*б*)

Table 2

Results of static tensile test

Таблица 2. **Результаты испытания на статическое растяжение**

State	Part of the wall	$\sigma_{0.2}$, MPa	σ_u, MPa	ε, %
09G2S substrate	–	280 ± 7	440 ± 8	28 ± 3
ER70S-6 (reference data)	–	–	480 – 550	22 – 30
GMAW	upper (zone *3*)	260 ± 9	422 ± 11	26 ± 2
	lower (zone *2*)	340 ± 10	472 ± 10	28 ± 3
	vertical section	265 ± 11	428 ± 12	20 ± 2

Samples cut from zone *2* and the substrate demonstrate a wide yield plateau, whereas samples from zone *3* and the vertical wall section have a much smaller yield plateau. The samples from the vertical wall section fail at the weakest point of the sample corresponding to zone *3*, aligning with the calculated tensile strength in these regions of the wall.

Results and discussion

Layer-by-layer printing of products induces cyclic heating and multiple phase transformations of underlying layers [11]. With an increase in the number of 3D printing passes, heat accumulates in the wall, and the cooling rate decreases. Over time, during the deposition of a new layer, excessive spreading and distortion occur due to heat accumulation in the wall. This "critical" heat accumulation begins approximately in the middle of the wall, where undulating layer boundaries are clearly visualized. A similar effect observed in 3D wall printing is discussed in [9].

The structure in zone *1* originated from the specific conditions during deposition of the first layers on the substrate. The 3D printing of the wall initiated at room temperature and was performed on a substrate mounted on a solid metal table. This setup significantly enhances heat removal for the initial wall layers, resulting in a high crystallization rate and a significant thermal gradient, facilitating the epitaxial growth of austenitic grains (Fig. 2, *d*) [12]. The formation of allotriomorphic ferrite along the boundaries of former austenitic grains suggests the occurrence of partial diffusion processes. However, acicular ferrite is formed internally, representing a structure of intermediate bainitic transformation, typical in welds [13]. A similar pattern of structure formation during 3D printing of walls is discussed in [7; 14 – 16].

For subsequent layers, heat removal was reduced, both due to substrate heating and a decrease in the contact area with the substrate. Consequently, during 3D printing, with the deposition of each new layer, the underlying layers experience overheating, resulting in recrystallization. Dispersed polygonal ferrite grains and granular pearlite are also formed (Fig. 2, *i*). Granular pearlite is formed due to cyclic heating of layers and insufficient holding time, limiting the time for adequate austenite homogenization.

The upper part of the wall (zone 3), being formed at higher heating temperatures affecting the underlying layers, reduced cooling rates, and sufficient homogenization of austenite, exhibits a predominantly ferrite-sorbitic structure with a small proportion of Widmanstatten and acicular ferrite. Similar results were demonstrated in [17; 18]. However, as the number of layers increases, and hence the heat build-up in the wall, the size of ferrite grains also increases (up to 29.8 ± 2 μm). The very last layers of the wall, due to direct contact with the atmosphere, cool at a higher rate and do not recrystallize as a result of reheating from the following layers [19], resulting in fewer sorbitic regions and a larger proportion of the bainitic component (Widmanstatten and acicular ferrite). This accounts for the less pronounced yield plateau of samples from zone 3 and the vertical wall section. Previous studies have shown that when more than 20 % of the bainite phase is present in the structure of low-carbon steel, the yield plateau in the tension graph completely disappears [20]. Another reason for the shorter yield plateau may be the coarse-grained structure, as fine-grained steels are known to have a longer yield plateau and higher yield strength due to a larger number of contact resistances at grain boundaries compared to coarse-grained steels. The inhomogeneous deformation on the parabolic part of the load curve of the sample from the vertical section may be related to its having an inhomogeneous structure, as it was cut from the wall region containing zones *2* and *3*.

Changes in microstructure along the wall height correlate with with variations in microhardness (Fig. 3, *a*). Microhardness decreases in the heat-affected zone of the substrate material due to several reasons. As the first layers form with short-term substrate heating, the material undergoes tempering, and granular pearlite is formed. The microhardness in zone *1* increases (up to about 1.8 GPa) due to the formation of the acicular ferrite structure. Residual stresses resulting from abrupt

heat removal [19] can also contribute to the increase in microhardness.

In zone *2*, microhardness gradually decreases as the ferrite-perlite structure forms, and the grain sizes increase from 11 ± 1 to 16.3 ± 2 μm due to heat accumulation during layer deposition and a lower cooling rate. Microhardness in zone *3* further decreases (to 1.3 GPa) owing to an increase in the average grain size to 29.8 ± 2 μm. Closer to the top of the wall, corresponding to the last deposited layers, microhardness increases (from 1.3 to 1.5 GPa) due to a higher cooling rate and an increase in the proportion of Widmanstatten and acicular ferrite. The boundary of this transition corresponds to a depth of 4 mm from the top of the wall (zone *3*) and is accompanied by a large spread of microhardness values. This is because structures with very different microhardness values are formed, such as large ferrite grains and regions of acicular ferrite.

Thus, the most uniform level of microhardness values and the most optimal mechanical characteristics are observed in zone *2*. As the wall sections are formed, the main issues causing increased microhardness (zone *1*) or, on the contrary, decreased values of this parameter (zone *3*) are the excessively high cooling rate due to the rapid heat removal to the substrate or severe overheating in the upper part of the wall due to low heat removal. Possible solutions to these problems may include, firstly, substrate preheating aimed at reducing the cooling rate in the first layers, and secondly, an increase in the time interval before depositing each layer to allow the previously formed layers to cool to the specified temperature.

Conclusions

We investigated the structure and mechanical properties of the steel wall produced using the electric arc additive technology (WAAM) with ER70S-6 wire on the substrate made of 09G2S steel.

Due to the rapid heat removal to the substrate during the initial stages of 3D printing, large austenitic grains with a columnar shape are formed in the structure of the wall base (zone *1*). Along the grain boundaries, allotriomorphic ferrite is released during rapid cooling, and within them, bainite transformation occurs, leading to the formation acicular ferrite. This type of structure is characterized by the highest microhardness values (up to 1.8 GPa).

The middle part of the wall (zone *2*) consists of ferrite grains (11 ± 1 to 16.3 ± 2 μm in size) with inclusions of granular pearlite. This dispersed structure is formed through recrystallization during cyclic heating and a decrease in the cooling rate caused by heat accumulation during multiple 3D printing passes. The formation of this structure results in lower microhardness in zone *2* (up to 1.3 GPa) compared to microhardness in zone *1*. The increased values of accumulated heat and overheating in the upper zones of the wall lead to excessive "spreading" of the forming layers and formation of undulating boundaries (zone *3*).

High temperatures and low cooling rates result in the formation of a coarse-grained structure (with a grain size up to 29.8 ± 2 μm), including sections of ferrite and sorbite with inclusions of Widemanstatten and acicular ferrite. Consequently, the microhardness decreases to 1.3 GPa in this zone.

Static tensile tests revealed anisotropy in the mechanical properties of the wall material in different directions relative to 3D printing. The best mechanical properties were recorded in the lower part of the wall (zone *2*) for the samples cut in the horizontal direction ($\sigma_{0.2}$ = 340 MPa, σ_u = 470 MPa). The samples cut in the vertical direction relative to 3D printing from zone *3* exhibited the worst strength characteristics ($\sigma_{0.2}$ = 260 MPa, σ_u = 425 MPa).

References / Список литературы

1. Gibson I., Rosen D., Stucker B. *Additive Manufacturing Technologies: 3D Printing, Rapid Prototyping, and Direct Digital Manufacturing*. NY: Springer New York; 2015:498. https://doi.org/10.1007/978-1-4939-2113-3
2. Senthil T.S., Babu S.R., Puviyarasan M., Dhinakaran V. Mechanical and microstructural characterization of functionally graded Inconel 825-SS316L fabricated using wire arc additive manufacturing. *Journal of Materials Research and Technology*. 2021;15:661–669. https://doi.org/10.1016/j.jmrt.2021.08.060
3. Jafari D., Vaneker T.H.J., Gibson I. Wire and arc additive manufacturing: Opportunities and chellenges to control the quality and accuracy of manufactured parts. *Materials & Design*. 2021;202:109471. https://doi.org/10.1016/j.matdes.2021.109471
4. Buchanan C., Gardner L. Metal 3D printing in construction: A review of methods, research, applications, opportunities and challenges. *Engineering Structures*. 2019;180:332–348. http://doi.org/10.1016/j.engstruct.2018.11.045
5. Lin Z., Song K., Yu X. A review on wire and arc additive manufacturing of titanium alloy. *Journal of Manufacturing Processes*. 2021;70:24–45. https://doi.org/10.1016/j.jmapro.2021.08.018
6. Wu B., Ding D., Pan Z., Cuiuri D., Li H., Han J., Fei Z. Effects of heat accumulation on the arc characteristics and metal transfer behavior in wire arc additive manufacturing of Ti6Al4V. *Journal of Materials Processing Technology*. 2017;250:304–312. http://doi.org/10.1016/j.jmatprotec.2017.07.037
7. Shamsujjoha M., Licavoli J., Lin B., Harma E., Patterson R., Timmermann T., Groeneveld M., McLeod L., Sanders P. Tailoring microstructure of wire arc additively manufactured C–Mn–Si steel with post process heat treatment. *Materials Science and Engineering: A*. 2021;825:141921. https://doi.org/10.1016/j.msea.2021.141921

8. Astafurova E.G., Astafurov S.V., Revunova K.A., Mel'nikov E.V., Moskvina V.A., Panchenko M.V., Maier G.G., Rubtsov V.E., Kolubaev E.A. Regularities of structure formation in chromium-manganese vanadium-containing steel with a high concentration of C + N = 1,9 wt. % in electron beam additive manufacturing. *Fizicheskaya mezomekhanika*. 2021;24(3):5–16. (In Russ.). https://doi.org/10.24412/1683-805X-2021-3-5-16

Астафурова Е.Г., Астафуров С.В., Ревунова К.А., Мельников Е.В., Москвина В.А., Панченко М.В., Майер Г.Г., Рубцов В.Е., Колубаев Е.А. Закономерности формирования структуры в хромомарганцевой ванадийсодержащей стали с высокой концентрацией атомов внедрения C + N = 1,9 мас. % при электронно-лучевом аддитивном производстве. *Физическая мезомеханика*. 2021;24(3):5–16. https://doi.org/10.24412/1683-805X-2021-3-5-16

9. Huang C., Kyvelou P., Zhang R., Ben Britton T., Gardner L. Mechanical testing and microstructural analysis of wire arc additively manufactured steels. *Materials & Design*. 2022;216:110544. https://doi.org/10.1016/j.matdes.2022.110544

10. Sun L., Jiang F., Huang R., Yuan D., Guo C., Wang J. Anisotropic mechanical properties and deformation behaviour of low-carbon high-strength steel component fabricated by wire and arc additive manufacturing. *Materials Science and Engineering: A*. 2020;787:139514. http://dx.doi.org/10.1016/j.msea.2020.139514

11. Panchenko O., Kladov I., Kurushkin D., Zhabrev L., Ryl'kov E., Zamozdra M. Effect of thermal history on microstructure evolution and mechanical properties in wire arc additive manufacturing of HSLA steel functionally graded components. *Materials Science and Engineering: A*. 2022;851:143569. https://doi.org/10.1016/j.msea.2022.143569

12. Razumov I.K., Gornostyrev Yu.N., Katsnelson M.I. Towards the ab initio based theory of phase transformations in iron and steel. *Physics of Metals and Metallography*. 2017; 118(4):362–388. https://doi.org/10.1134/S0031918X16130032

Разумов И.К., Горностырев Ю.Н., Кацнельсон М.И. К теории фазовых превращений в железе и стали на основе первопринципных подходов. *Физика металлов и металловедение*. 2017;118(4):380–408. https://doi.org/10.7868/S001532301704009X

13. Lan L., Kong X., Qiu C., Zhao D. Influence of microstructural aspects on impact toughness of multi-pass submerged arc welded HSLA steel joints. *Materials & Design*. 2016;90:488–498. https://doi.org/10.1016/j.matdes.2015.10.158

14. Anand M., Kumar Das A. Grain refinement in wire-arc additive manufactured Inconel 82 alloy through controlled heat input. *Journal of Alloys and Compounds*. 2022; 929:166949. https://doi.org/10.1016/j.jallcom.2022.166949

15. Yehorov Y., Da Silva L.J., Scotti A. Exploring the use of switchback for mitigating homoepitaxial unidirectional grain growth and porosity in WAAM of aluminium alloys. *The International Journal of Advanced Manufacturing Technology*. 2019;104(1-4):1581–1592. https://doi.org/10.1007/s00170-019-03959-w

16. Basak A., Das S. Epitaxy and microstructure evolution in metal additive manufacturing. *Annual Review of Materials Research*. 2016;46:125–149. https://doi.org/10.1146/annurev-matsci-070115-031728

17. Aldalur E., Veiga F., Suárez A., Bilbao J., Lamikiz A. High deposition wire arc additive manufacturing of mild steel: Strategies and heat input effect on microstructure and mechanical properties. *Journal of Manufacturing Processes*. 2020;58:615–626. https://doi.org/10.1016/j.jmapro.2020.08.060

18. He J., Feng X., Wang X., Guan X. Fatigue performance and acoustic emission behavior of remanufactured low-carbon steel made by wire and arc additive manufacturing. *International Journal of Fatigue*. 2022;165:107190. https://doi.org/10.1016/j.ijfatigue.2022.107190

19. Rani K.U., Kumar R., Mahapatra M.M., Mulik R.S., Świerczyńska A., Fydrych D., Pandey C. Wire arc additive manufactured mild steel and austenitic stainless steel components: Microstructure, mechanical properties and residual stresses. *Materials*. 2022;15(20):7094. https://doi.org/10.3390/ma15207094

20. Efron L.I. *Metals Science in Big Metallurgy: Pipe Steels*. Moscow: Metallurgizdat; 2012:694. (In Russ.).

Эфрон Л.И. *Металловедение в большой металлургии: Трубные стали*. Москва: Металлургиздат; 2012:694.

Information about the Authors / Сведения об авторах

Il'ya V. Vlasov, *Cand. Sci. (Eng.), Research Associate of the Laboratory of Physical Mesomechanics and Non-Destructive Testing,* Institute of Strength Physics and Materials Science, Siberian Branch Russian Academy of Sciences
ORCID: 0000-0001-9110-8313
E-mail: viv@ispms.ru

Илья Викторович Власов, *к.т.н., научный сотрудник лаборатории физической мезомеханики и неразрушающих методов контроля,* Институт физики прочности и материаловедения Сибирского отделения РАН
ORCID: 0000-0001-9110-8313
E-mail: viv@ispms.ru

Antonina I. Gordienko, *Cand. Sci. (Eng.), Research Associate of the Laboratory of Physical Mesomechanics and Non-Destructive Testing,* Institute of Strength Physics and Materials Science, Siberian Branch Russian Academy of Sciences
ORCID: 0000-0002-4361-8906
E-mail: mirantil@ispms.ru

Антонина Ильдаровна Гордиенко, *к.т.н., научный сотрудник лаборатории физической мезомеханики и неразрушающих методов контроля,* Институт физики прочности и материаловедения Сибирского отделения РАН
ORCID: 0000-0002-4361-8906
E-mail: mirantil@ispms.ru

Anastasya E. Kuznetsova, *Postgraduate, Junior Researcher of the Laboratory of Structural Design and Advanced Materials,* Institute of Strength Physics and Materials Science, Siberian Branch Russian Academy of Sciences
ORCID: 0000-0001-6966-8402
E-mail: aekuznetsova@ispms.ru

Анастасия Евгеньевна Кузнецова, *аспирант, младший научный сотрудник лаборатории структурного дизайна перспективных материалов,* Институт физики прочности и материаловедения Сибирского отделения РАН
ORCID: 0000-0001-6966-8402
E-mail: aekuznetsova@ispms.ru

Vyacheslav M. Semenchuk, *Junior Researcher of the Laboratory of Local Metallurgy in Additive Manufacturing Technologies,* Institute of Strength Physics and Materials Science, Siberian Branch Russian Academy of Sciences
ORCID: 0000-0002-7215-0505
E-mail: svm_70@ispms.ru

Вячеслав Максимович Семенчук, *младший научный сотрудник лаборатории локальной металлургии в аддитивных технологиях,* Институт физики прочности и материаловедения Сибирского отделения РАН
ORCID: 0000-0002-7215-0505
E-mail: svm_70@ispms.ru

Contribution of the Authors / Вклад авторов

I. V. Vlasov – formation of the main concept, goals and objectives; writing the text, literary review, data analysis.

A. I. Gordienko – results processing, data analysis, revising the text.

A. E. Kuznetsova – conducting experimental studies, results processing, data analysis.
V. M. Semenchuk – selection of additive manufacturing modes, results discussion.

И. В. Власов – формирование основной концепции, цели и задач исследования; написание текста статьи, литературный обзор публикаций по теме, анализ экспериментальных данных.
А. И. Гордиенко – обработка результатов и анализ данных, доработка текста.
А. Е. Кузнецова – проведение экспериментальных исследований, обработка результатов и анализ данных.
В. М. Семенчук – подбор режимов проведения аддитивнго формования, обсуждение полученных результатов.

Received 27.04.2023
Revised 13.06.2023
Accepted 11.09.2023

Поступила в редакцию 27.04.2023
После доработки 13.06.2023
Принята к публикации 11.09.2023